Cooling System Design Optimization of an Enclosed PM Traction Motor for Subway Propulsion Systems

Longnv Li, *Member, IEEE*, Nan Jia, Xizhe Wang, Yiran Yun, and Gaojia Zhu, *Member, IEEE*

***Abstract*—This paper presents the design optimization of a self-circulated ventilation system for an enclosed permanent magnet (PM) traction motor utilized in the propulsion systems for subway trains. In order to analyze accurately the machine's inherent cooling capacity when the train is running, the ambient airflow and the related heat transfer coefficient (HTC) are numerically investigated considering synchronously the bogie installation structure. The machine is preliminary cooled with air ducts set on the motor shell, and the fluidic-thermal field distributions with only the shell air duct cooling are numerically calculated. During simulations, the HTC obtained in the former steps is applied to the external surface of the machine to model the inherent cooling characteristic caused by the train movement. To reduce the temperature rise and thus guarantee the motor's working reliability, an internal self-circulated air cooling system is proposed according to the machine temperature distribution. The air enclosed in the end-caps is driven by the blades mounted on both sides of the rotor core and forms two air circuits to bring the excessive power losses generated in the heating components to cool regions. The fluid flow and temperature rise distributions of the cooling system's structural parameters are further improved by the Taguchi method in order to confirm the efficacy of the internal air cooling system.**

***Index Terms*—Permanent magnet (PM) traction motor, Bogie installation structure, Self-circulated ventilation system, Taguchi method.**

I. Introduction

ELECTRIC drives have attracted extensive research and manufacturing attentions in railway transportation systems owing to their advantages of high reliability, energy-saving, and high controllability. To further improve the power densities and efficiencies of the systems, permanent magnet synchronous machines (PMSMs) have been widely applied as traction motors for their superior characteristics of high power (torque) density, wide high-efficiency range, and fast dynamics [1]-[2]. However, since permanent magnet (PM) traction machines are generally supplied with PWM power converters, the high-frequency harmonics can generate excessive eddy currents and thus elevate seriously the motor temperature rises. The high temperature rises will result in insulation failures and even cause the demagnetization of the PMs [3]-[4]. In order to maintain the machines' operational dependability and output capacity, it is crucial to design and develop effective cooling methods for PM traction motors.

Among the cooling systems for traction motors, liquid cooling (direct or indirect) is most commonly utilized for its excellent heat dissipation capacity [5]-[7]. In [5], Zhang *et al*, proposed the design optimization of water jackets from thermal, fluidic, and mechanical perspectives. A method for designing active cooling systems was created by Roy *et al* [6], and the design optimization of a circumferential cooling jacket for a PMSM is carried out. For a tooth coil winding machine, Acquaviva *et al*, [7] presented an in-slot and in-stator direct oil cooling system that achieves cooling system integration. Experiments are used to confirm the system's viability.

However, as the cooling and maintenance costs for liquid cooling systems are relatively high, air-ventilated structures with open or enclosed structures have been widely employed. Jercic *et al*, [8] describe a two-stage design for a centrifugal fan mounted on a motor shaft. The fundamental fan sizing is determined by analytical formulas, and it is then decided based on CFD analysis. The maximum PMs temperature rise and air resistance loss are explored using the Taguchi technique at three operating settings thanks to a novel inclined flow deflector devised by Kang *et al*, [9] and used in the rotor end spider. In [10], Zhu *et al*, presented a hybrid ventilation system for PMSMs with clapboards inside the radial vents to drive the cooling airflow. Since the width of the clapboards working as the centrifugal blades are limited by the radial vent width, the cooling effect is thus restricted.

To maximize the heat dissipation capacities, several optimization methods are employed in designing cooling systems for electrical machines. Ulbrich *et al*, [11] established a 2D model to illustrate the heat transfer characteristics of cooling fins mounted on the casing of an enclosed machine, and the number and sizes of the fins are optimized using a

Manuscript received February 10, 2023; revised March 05, 2023; accepted March 23, 2023. Date of publication December 25, 2023. Date of current version June 14, 2023.

This work was supported by the National Natural Science Foundation of China under Grant 52107007, the China Scholarship Council under Grant 202008120084, and the "Chunhui Plan" Collaborative Research Project of Chinese Ministry of Education under Grant HZKY20220604. (*Corresponding Author*: *Gaojia Zhu*)

Longnv Li, Xizhe Wang, and Gaojia Zhu are with the School of Electrical Engineering, Tiangong University, Tianjin 300387, China; and G. J. Zhu is also with the Power Electronics, Machines and Control Research Group, University of Nottingham, Nottingham NG7 2RD, U K (e-mail: lilongnv@tiangong.edu.cn, 1515675488@qq.com, zhugaojia@tiangong.edu.cn).

Nan Jia is with Tangshan Fengnan District Power supply Branch, State Grid Jibei Electric Power Co. Ltd., Tangshan 063000, China (e-mail: 1131615408@qq.com).

Yiran Yun is with State Grid Tianjin Ninghe Electric Power Supply Company, Tianjin, China (e-mail: A26A46@163.com).

Digital Object Identifier 10.30941/CESTEMS.2023.00037

DE/rand/1/bin evolutionary algorithm. Zhang *et al*, [12] optimized the structures of a water-cooled heat sink for a motor controller based on a fruit fly optimization algorithm. The effectiveness of the optimal results is validated through experiments. However, as the numerical modelings of conjugate heat transfer problems are computationally costly, the Taguchi method with excellent optimization efficiency has been extensively utilized [13]. Wang *et al*, [14] used the Taguchi method to optimize the sizes of an oil injection system for a PMSM. In [4], the structural parameters of a self-circulated oil cooling system are optimized through Taguchi analyses.

In this paper, an enclosed self-circulated ventilation system is proposed for the efficient cooling of a PM traction motor. First, the inherent cooling ability of the machine considering the installation structure and the external air flow conditions is numerically analyzed and modeled through a heat transfer coefficient (HTC). The temperature rise and fluid flow distributions inside the machine are then simulated considering synchronously the inherent external cooling capacity. Based on the calculation results, a novel self-circulated air ventilation system is established for a PM traction motor. The Taguchi approach is then used with comparative analyses to optimize the cooling structural factors. Temperature rise calculation results show that, after optimizing the control factors of the cooling system, the temperature rise of the machine can be effectively reduced.

II. Inherent Cooling Capacity Investigation

A. Traction Motor Installation Structure

Since the traction motor studied in this paper is installed in the bogies of a subway train, the temperature and fluid flow fields are firstly analyzed to get the heat dissipation capacities of the motor exterior surfaces. The three-dimensional (3D) physical model of the bogie is shown in Fig. 1. Fig. 2 illustrates the windward side and leeward side definitions of the traction motor.

B. Boundary Conditions

The following boundary conditions are applied during simulations [15]-[16]:

1) To simulate the motion of the subway train, a velocity inlet boundary, and a pressure outlet boundary are used.

2) The κ-ε turbulence model is used in the computations

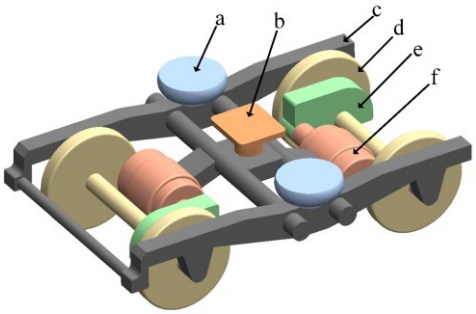

Fig. 1. 3D physical model of the subway bogie, where (a) secondary suspension, (b) traction instrument, (c) frame, (d) wheelset, (e) gear container, and (f) PM traction motor.

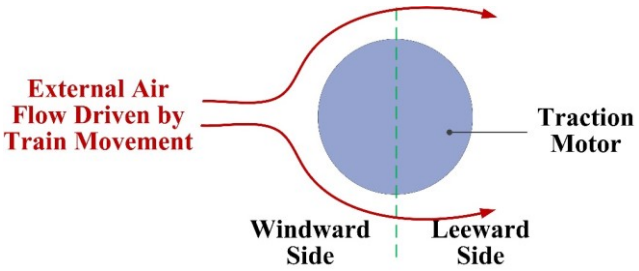

Fig. 2. Schematic diagram of the windward side and the leeward side.

since the air is in a turbulent state with a high Reynolds number (*Re*) due to the train's comparatively high speed (at 22.22 m/s).

3) The air is thought to be incompressible since the velocity is much lower than the sonic speed.

C. Calculations and Discussions

Fig. 3 is the velocity vector of the overall bogie. Fig. 4 is the velocity streamline of the *Z*=1. 65 m section plane. It can be seen that the vortex appears on the leeward side of the motor, which is not conducive to heat dissipation.

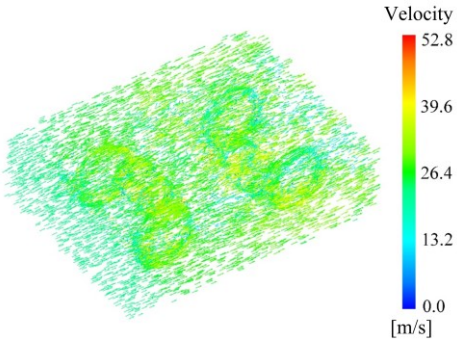

Fig. 3. Velocity vector of the bogie.

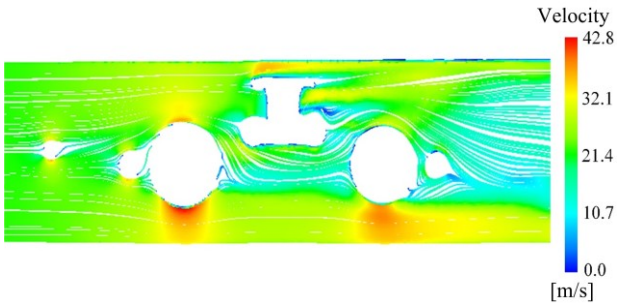

Fig. 4. Velocity streamline of Z=1.65 m section plane.

Fig. 5 shows the heat transfer coefficient distribution on the windward and leeward sides of the front motor, and Fig. 6 shows the rear motor. The lowest heat transfer coefficient appears on the leeward side of the rear motor, and both motors have better heat dissipation effects on the windward than on the leeward side.

III. Fluidic-thermal Investigation with Preliminary Cooling Structure

A. Motor Structure

The fundamental design of the motor under study in this paper is depicted in Fig. 7. The PMs are placed in a "V" form

and have a 6-pole rotor. The motor uses an external fan-blowing cooling system with train movement-driven exterior ventilation. In Table I, the motor parameters are displayed.

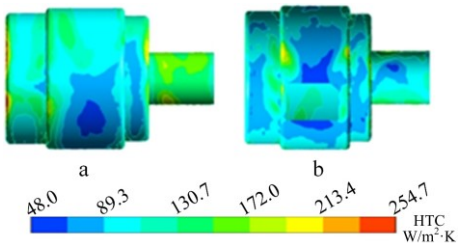

Fig. 5. Heat transfer coefficient distribution on the windward and leeward side of the front motor, where (a) windward side, (b) leeward side.

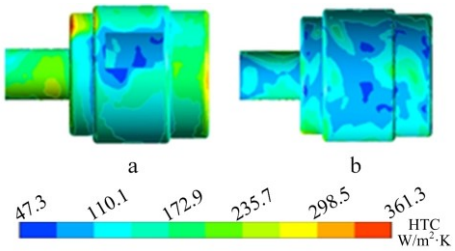

Fig. 6. Heat transfer coefficient distribution on the windward and leeward side of the rear motor, where (a) windward side, (b) leeward side.

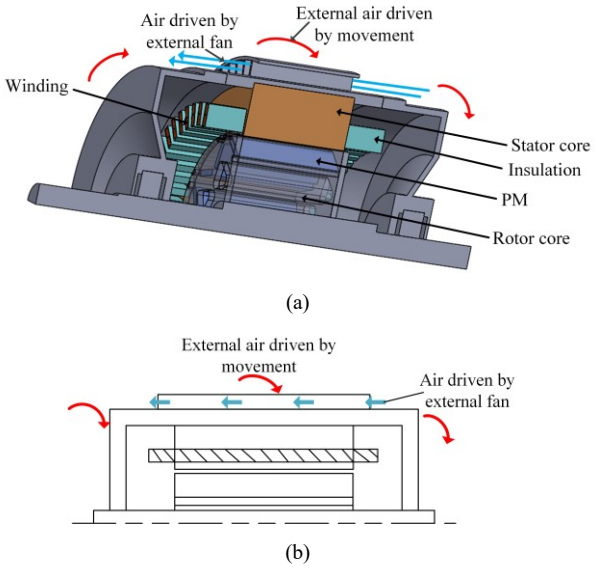

Fig. 7. PM traction motor. (a) Basic structure. (b) Preliminary cooling structure.

TABLE I
BASIC PARAMETERS OF THE MOTOR

Quantity	Value
Rated Power/kW	170
Rated Speed/(r/min)	1800
Maximum Speed/(r/min)	3600
Stator Core Outer Diameter/mm	460
Stator Core Inner Diameter/mm	320
Air Gap Length/mm	1.5
Number of Rotor Vents	6

B. Fluidic-thermal Analyses

A numerical investigation is done into the machine's temperature rise when it is running at its maximum speed. The distribution of the machine's temperature rise is shown in Fig. 8. The end-windings, which are shown in Fig. 9, exhibit the largest temperature rise with a value of 201.82 K, as is evident from the figure. The core region of the PMs experiences the largest temperature rise, which is 132.38 K, as seen in Fig. 10.

It can be seen from the above calculation results that the working temperature of the PMs is about 160 ℃, and the end of windings close to the outlet of external airflow has a higher temperature rise. The overall temperature rise of the motor is too high to guarantee working reliability. In addition, the distribution of temperature rise is extremely uneven. Therefore, it is necessary to design an efficient internal self-circulation cooling system for the machine.

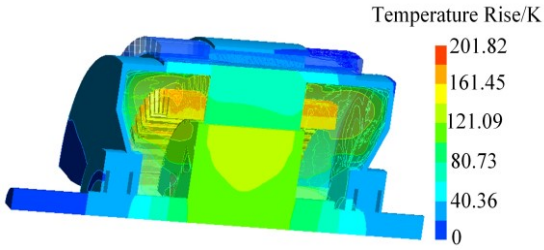

Fig. 8. Machine temperature rise with original external cooling structure.

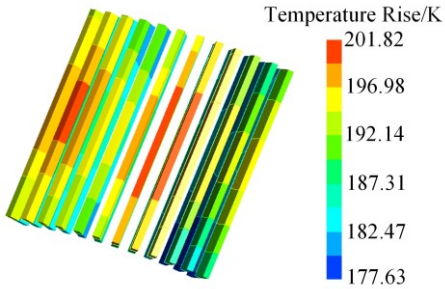

Fig. 9. Temperature rise of the windings.

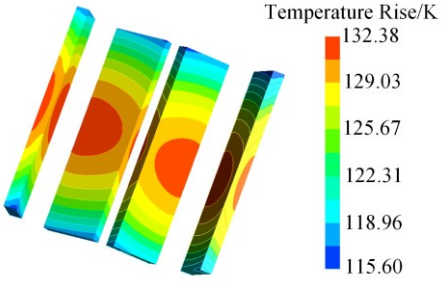

Fig. 10. Temperature rise of the PMs.

C. Validation

The temperature rise experiments are conducted on a 2.1 kW PMSM prototype with a very comparable cooling system in order to confirm the accuracy of the numerical investigation. The experimental platform is depicted in Fig. 11. PT100 thermal-sensitive resistors are used to measure the temperature of the end-windings, and an infrared radiation thermometer is utilized to detect the temperature of the shell surface.

3D fluidic-thermal coupled analyses are also performed on the 2.1 kW tested motor, the comparison between the experimental and numerical calculation results is listed in Table

II. It is evident that the temperature rise calculation errors can all be kept to 2% or less, demonstrating the correctness of the fluidic-thermal-based calculation results.

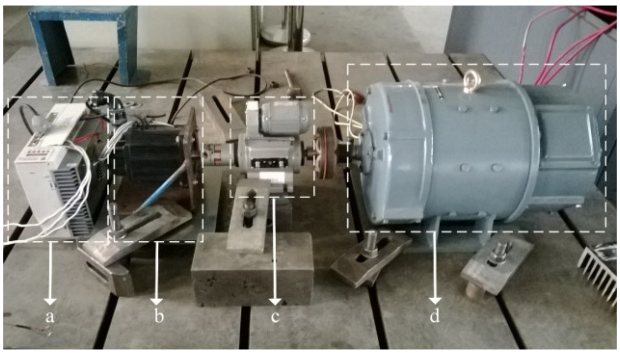

Fig. 11. Experimental platform, where (a) converter, (b) 2.1 kW tested motor, (c) torque and speed measurement instrument, (d) load machine.

TABLE II
COMPARISON BETWEEN EXPERIMENTAL AND CALCULATED RESULTS

Position	Measured (K)	Calculated (K)	Error (%)
End-winding	82.9	84.4	1.8
Shell	74.7	74.9	0.3

IV. SELF-CIRCULATED ENCLOSED COOLING SYSTEM DESIGN

A. Cooling Structure

To improve the heat dissipation capacity, and balance the temperature rise inside the motor, a self-circulated totally enclosed cooling structure shown in Fig. 12 is established. The rotor core, stator core, and PM are divided into two symmetrical parts. The centrifugal fan blades are mounted in the rotor end spider. The blades rotating with the rotor can increase air turbulence and generate pressure differences on the two sides of the rotor.

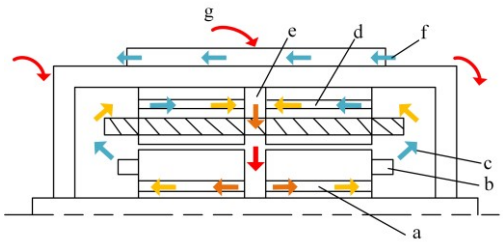

Fig. 12. Self-circulated totally enclosed cooling structure, where (a) axial rotor vents, (b) centrifugal fan, (c) internal cooling air, (d) axial stator vents, (e) radial vent, (f) air driven by an external fan, and (g) external air driven by train movement.

B. Cooling Effect Verification

CFD simulation is performed for the motor with the new cooling structure at the maximum speed operating state to confirm the cooling capacity of the self-circulated entirely enclosed cooling structure. The leeward side of the rear motor has the worst heat dissipation, according to simulation results from the bogie, and to verify the cooling effect, an application scenario with poor cooling conditions should be taken into account. As a result, the motor's wall heat transfer coefficient can be set to 90 W/(m^{2}K). The exterior air path's velocity-inlet is set to 15 m/s. The spread of the machine's temperature rise is shown in Fig. 13. The winding sections show a maximum temperature rise of 88.25 K. The distribution of temperature rise in the windings and PMs are depicted in Fig. 14 and 15, respectively.

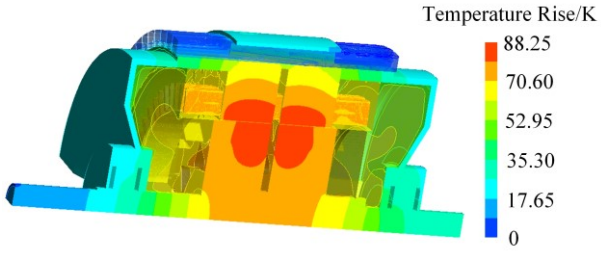

Fig. 13. Temperature rise of the whole machine.

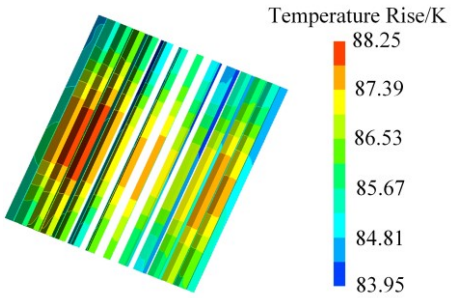

Fig. 14. Temperature rise of the wingdings.

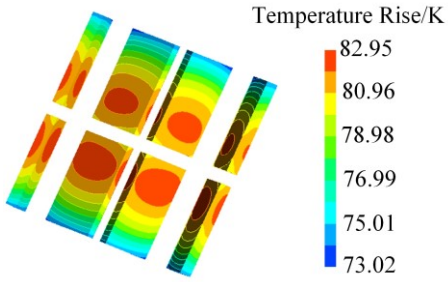

Fig. 15. Temperature rise of the PMs.

V. DESIGN OPTIMIZATION ON TAGUCHI METHOD

A. Design of Experiments

The Taguchi approach is used to reduce the number of experiments because the hybrid cooling system optimization design has numerous variables [17]-[18]. As seen in Fig. 16, the selected control parameters are the fan blades' width (w), height (h), angle (a) with respect to the radial direction, stator vent

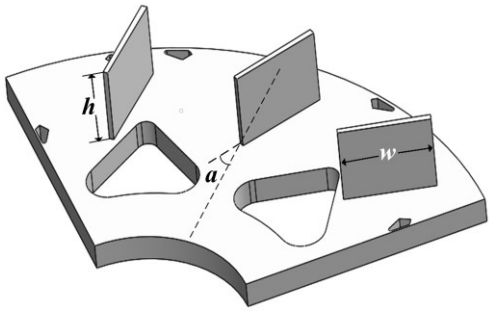

Fig. 16. Centrifugal fan blades.

diameter (*r*), and radial vent width (*d*).

The values range of the control variables can be established based on the motor's geometrical parameters. Table III provides the control factors and their levels. The highest PMs temperature rise T_{PM} and the highest windings temperature rise T_W are among the chosen optimization objectives.

TABLE III
FIVE CONTROL FACTORS AND THEIR LEVELS

Level	*w*/mm	*h*/mm	*a*/°	*r*/mm	*d*/mm
I	25	25	0	10	12.5
II	30	30	15	12.5	15
III	35	35	30	15	17.5
IV	40	40	45	17.5	20

B. Orthogonal Experiment and CFD Results

A conventional orthogonal array L16 (4^5) is built based on the number of the control variables and the number of their levels, as shown in Table IV. CFD is used to compute the maximum temperature rise of the PMs and windings in each experiment under the conditions of maximum speed operation.

TABLE IV
EXPERIMENT MATRIX AND RESULTS

No.	*w*	*h*	*a*	*r*	*d*	T_{PM}/K	T_W/K
1	25	25	0	10	12.5	81.56	87.49
2	25	30	15	12.5	15	80.12	86.16
3	25	35	30	15	17.5	80.26	90.22
4	25	40	45	17.5	20	76.44	81.31
5	30	25	15	15	20	78.73	81.47
6	30	30	0	17.5	17.5	76.52	85.08
7	30	35	45	10	15	82.62	87.42
8	30	40	30	12.5	12.5	78.51	81.28
9	35	25	30	17.5	15	82.87	88.77
10	35	30	45	15	12.5	82.95	88.25
11	35	35	0	12.5	20	72.53	81.30
12	35	40	15	10	17.5	73.90	83.25
13	40	25	45	12.5	17.5	73.13	80.04
14	40	30	30	10	20	70.34	78.97
15	40	35	15	17.5	12.5	72.21	77.84
16	40	40	0	15	15	72.60	82.27
Ave	-	-	-	-	-	77.21	83.82

C. Analyses and Discussions

1) Analysis of Mean

To examine the changes in the highest temperature rise of PMs and windings with changes in the amounts of each control factor, the mean for the CFD data is analyzed.

To begin with, the total mean m of the experimental outcomes shown in Table IV can be determined as follows:

$$m = \frac{1}{n}\sum_{i=1}^{n} m_i \tag{1}$$

where n is the number of experiments, and m_i is the experimental result of the i^{th} experiment.

Next, determine the average of the objective functions for each level of each control factor. The following equation will be used to compute the mean of the maximum PMs temperature rise under level I of factor *w*:

$$m_{T_{pm}}(w_1) = \frac{81.56 + 80.12 + 80.26 + 76.44}{4} = 79.60 \tag{2}$$

Similarly, the mean of objective functions under each level of the other four factors can be obtained respectively. Factors response graphs are shown in Fig. 17 and 18.

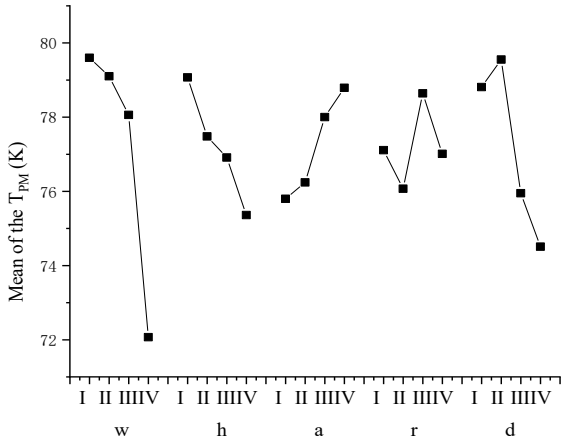

Fig. 17. Factors response graphs of the mean of T_{PM}.

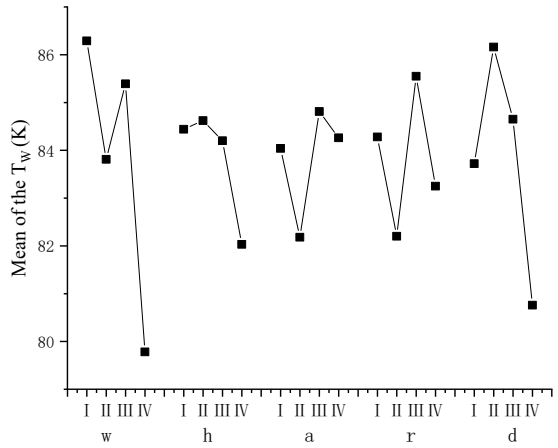

Fig. 18. Factors response graphs of the mean of T_W.

With the increase of factors *w* and *h*, the temperature rise of PMs decreases monotonously, and the temperature rise of the windings generally shows a downward trend although there are fluctuations. The increase of factor *a* will reduce the convection effect at both ends of the cavity and weaken the cooling effect. The convection effect in the vents will be impacted by a change in the factor *r*, and the temperature rise of the PMs and windings will exhibit a decreasing, increasing, and then reducing trend. The temperature rise can be lowered by widening the radial vent, however, factor *d* shouldn't be set too high to prevent the machine from becoming overly huge.

The optimal combination of the level taken by each control factor is *w*(IV) *h*(IV) *a*(I) *r*(II) *d*(IV), which makes the T_{PM} smallest. And the combination making the T_W smallest is *w*(IV) *h*(IV) *a*(II) *r*(II) *d*(IV).

2) Analysis of Variance

The analysis of variance for the CFD results is also performed to analyze the relative importance of five control factors on the two optimization objectives. The expression of variance is shown as:

$$S_A = \frac{1}{4}\sum_{j=1}^{4}\left[m_{A(j)} - m\right]^2 \tag{3}$$

where A represents the factors, $m_{A(j)}$ is the mean of T_{PM} or T_W under level j of factor A, the results are listed in Table V.

TABLE V
CALCULATION RESULTS OF THE VARIANCE

Factor	T_{PM}		T_W	
	S	Proportion	S	Proportion
w	9.11	52.17%	6.23	45.41%
l	1.76	10.08%	1.09	7.94%
a	1.51	8.65%	0.98	7.15%
r	0.85	4.87%	1.54	11.22%
d	4.23	24.23%	3.88	28.28%

D. Determination of Optimal Scheme

In two optimization combinations, factor *a* is chosen at various levels based on the mean and variance analysis. The variation of factor *a* for the maximum temperature increase in the PMs is greater than that for the highest temperature increase in the windings. The control factors level combination is *w*(IV) *h*(IV) *a*(I) *r*(II) *d*(IV), and the value of each parameter is 40 mm, 40 mm, 0°, 12.5 mm, 20 mm. CFD is used to simulate the motor's temperature field after optimization. The distribution of temperature rise for the entire machine, the windings, and the PMs are shown in Fig. 19, 20, and 21, respectively. The highest winding and PM temperature rises are 77.23 K and 70.99 K, respectively, as shown by the figures. The internal air ventilation system effectively lowers the machine's winding and PM temperature rises, as can be shown by comparing Fig. 20~21 to Fig. 14~15.

The detailed comparisons are demonstrated in Fig. 22.

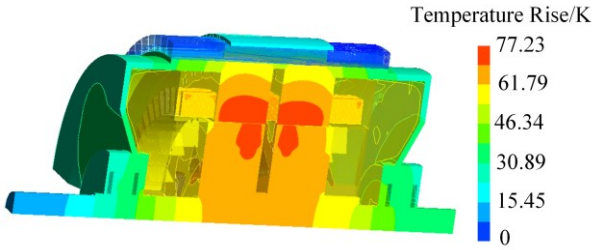

Fig. 19. Temperature rise of optimized machine.

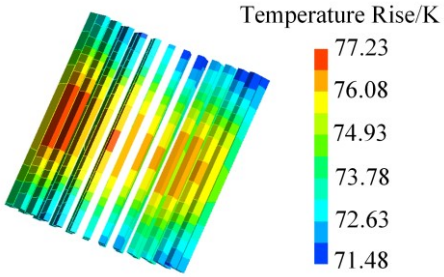

Fig. 20. Temperature rise of the wingdings.

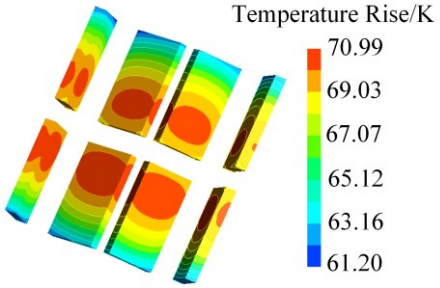

Fig. 21. Temperature rise of the PMs.

Compared with the original structure, the highest winding temperature rise of the self-circulated totally-enclosed cooling structure is decreased by 56.27%, and the highest PM temperature rise is decreased by 37.34%. After optimization, the T_W decreased by 12.49%, and the T_{PM} decreased by 14.42%.

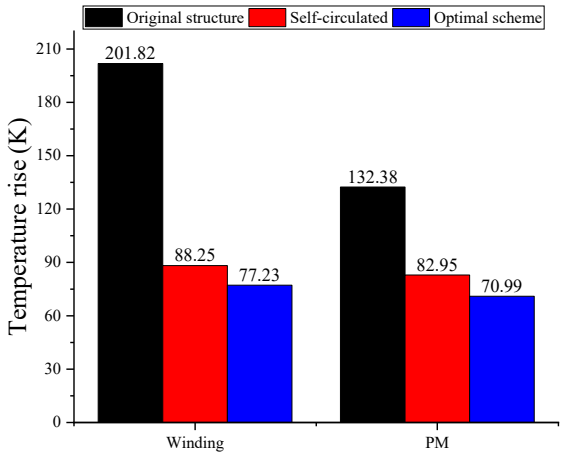

Fig. 22. Comparison of the highest temperature rise of three structures.

VI. CONCLUSION

The installation structure and the external airflow brought on by the movement of the train are taken into consideration as this paper examines the inherent external cooling capability of a PM subway traction motor. Taking into account the inherent exterior cooling capacity, an enclosed self-circulated cooling structure is suggested. The self-circulated cooling system can successfully maintain and balance the motor's temperature rise, thus ensuring operational reliability. To achieve optimum cooling structure characteristics for greater cooling efficiency, the Taguchi method is used. Fluidic-thermal coupled analyses are used to validate the effectiveness of the cooling structure proposed and the optimizations.

REFERENCES

[1] X. D. Sun, T. Li, and Z. Zhu *et al*, "Speed Sensorless Model Predictive Current Control Based on Finite Position Set for PMSHM Drives," *IEEE Transactions on Transportation Electrification*, vol. 7, no. 4, 2743-2752, Dec. 2021.

[2] K. T. Chau, C. C. Chan, and C. Liu, "Overview of Permanent-Magnet Brushless Drives for Electric and Hybrid Electric Vehicles," *IEEE Transactions on Industrial Electronics*, vol. 55, no. 6, pp. 2246-2257, Jun. 2008.

[3] Q. Lu, Xinmin Zhang, and Yi Chen *et al*, "Modeling and Investigation of Thermal Characteristics of a Water-Cooled Permanent-Magnet Linear Motor," *IEEE Transactions on Industry Applications*, vol. 51, no. 3, pp. 2086-2096, May./Jun. 2015.

[4] G. J. Zhu, L. N. Li, and Y. H. Mei *et al*, "Design and Analysis of a Self-Circulated Oil Cooling System Enclosed in Hollow Shafts for Axial-Flux PMSMs," *IEEE Transactions on Vehicular Technology*, vol. 71, no. 5, pp. 4879-4888, May 2022.

[5] B. Zhang, R. Qu, and X. Fan *et al*, "Thermal and mechanical optimization of water jacket of permanent magnet synchronous machines for EV application," *in Proc. of 2015 IEEE International Electric Machines & Drives Conference (IEMDC)*, Coeur d'Alene, ID, USA, 2015, pp. 1329–1335.

[6] P. Roy, A. J. Bourgault, and M. Towhidi *et al*, "An algorithm for effective design and performance investigation of active cooling system for required temperature and torque of pm traction motor," *IEEE Transactions Magnetics*, vol. 57, no, 2, Feb. 2021.

[7] A. Acquaviva, S. Skoog, and T. Thiringer, "Design and Verification of

In-slot Oil-Cooled Tooth Coil Winding PM Machine for Traction Application," *IEEE Transactions on Industrial Electronics*, vol. 68, no. 5, pp. 3719-3727, May. 2021.
[8] T. Jercic, D. Zarko, and M. Martinovic *et al*, "Centrifugal fan design for permanent magnet synchronous motor in a traction application," in *Proc. of 2017 IEEE International Electric Machines and Drives Conference (IEMDC)*, Miami, FL, USA, 2017, pp. 1-7.
[9] M. Kang, H. Wang, and L. Guo *et al*, "Self-circulation cooling structure design of permanent magnet machines for electric vehicle," *Applied Thermal Engineering*, vol. 165, Jan. 2020, Art. no. 114593.
[10] G. Zhu, Y. Zhu, and W. Tong *et al*, "Double-Circulatory Thermal Analyses of a Water-Cooled Permanent Magnet Motor Based on a Modified Model," *IEEE Transactions on Magnetics*, vol. 54, no. 3, Mar. 2018.
[11] S. Ulbrich, J. Kopte, and J. Proske, "Cooling Fin Optimization on a TEFC Electrical Machine Housing Using a 2-D Conjugate Heat Transfer Model," *IEEE Transactions on Industrial Electronics*, vol. 65, no. 2, pp. 1711-1718, Feb. 2018.
[12] Z. Zhang, Y. F. Liu, and J. Y. Wang, "Optimal Design of Multi-channel Water Cooled Radiator for Motor Controller of New Energy Vehicle," *CES Transactions on Electrical Machines and Systems*, vol. 6, no. 1, pp. 87-94, Mar. 2022.
[13] Z. Shi, X. Sun, and Y. Cai *et al*, "Robust design optimization of a five-phase PM hub motor for fault-tolerant operation based on Taguchi method," *IEEE Transactions on Energy Conversion*, vol. 35, no. 4, pp. 2036-2044. Dec. 2020.
[14] H. M. Wang, X. C. Liu, and M. Kang *et al*, "Oil Injection Cooling Design for the IPMSM Applied in Electric Vehicles," *IEEE Transactions on Transportation Electrification*, vol. 8, no. 3, pp. 3427-3440. Sept. 2022.
[15] W. Chen, Y. N. Ju, and D. Yan *et al*, "Design and optimization of dual-cycled cooling structure for fully-enclosed permanent magnet motor," *Applied Thermal Engineering*, vol. 152, pp. 338-349, Apr. 2019.
[16] F. E. Camelli, G. Byrne, and R. Lohner, "Modeling subway air flow using CFD," *Tunnelling and Underground Space Technology*, vol. 40, pp. 20-31, July 2014.
[17] A. J. Sorgdrager, R. Wang, and A. Grobler, "Multi-Objective Design of a Line-Start PM Motor Using the Taguchi Method," *IEEE Transactions on Industry Applications*, vol. 54, pp. 4167-4176, Sep/Oct. 2018.
[18] X. D. Sun, Z. Shi, and J. G. Zhu, "Multiobjective design optimization of an IPMSM for EVs based on fuzzy method and sequential Taguchi method," *IEEE Transactions on Industrial Electronics*, vol. 68, no. 11, pp. 10592-10600, Nov. 2021.

Longnv Li (Member, IEEE) received her Ph.D. degree in electrical engineering from National Engineering Research Center for Rare-Earth Permanent Magnet Machines, Shenyang University of Technology, Shenyang, China, in 2016. She has been with the School of Electrical Engineering, Tiangong University, Tianjin, China, since then (appointed as a lecturer in 2016 and an associate professor in 2022). Her research interests are the multi-physics coupled analysis and optimal design of electrical machines, transformers, and power modules.

Nan Jia received the B.S. degree in electrical engineering from Hebei Normal University, Shijiazhuang, China, in 2019, and the M. E. degree in electrical engineering from Tiangong University, Tianjin, China, in 2022. She is currently with Tangshan Fengnan District Power supply Branch, State Grid Jibei Electric Power Co. Ltd., Tangshan, China. Her research interests are the multi-physics coupled analyses and optimal design of electrical machines.

Xizhe Wang received the Bachelor's degree in engineering from Qufu Normal University in 2020. He is currently pursuing his Master's degree in electrical engineering at School of Electrical Engineering, Tiangong University. His research interest is on the evaporation-cooled transformers.

Yiran Yun received the bachelor's degree in electrical engineering and automation from Tiangong in 2019. He has been engaged in the transformation operation and maintenance of Ninghe Power Supply Branch of State Grid Tianjin Electric Power Company, since then. At present, he is an assistant engineer.

Gaojia Zhu (Member, IEEE) received his Ph.D. degree in electrical engineering from National Engineering Research Center for Rare-Earth Permanent Magnet Machines, Shenyang University of Technology, Shenyang, China, in 2017. He has been with the School of Electrical Engineering, Tiangong University, Tianjin, China, since then (appointed as a lecturer in 2018 and an associate professor in 2023). He is currently also a postdoctoral visiting researcher with the Power Electronics, Machines and Control Research Group, University of Nottingham, Nottingham, U K. His research interests include the multi-physical analysis and multi-disciplinary design optimization of PMSMs and power modules.